Analysis of nucleation ability of cluster configurations with Monte Carlo simulations of argon

Joonas Merikanto,[a] Evgeni Zapadinsky, and Hanna Vehkamäki
Department of Physical Sciences, University of Helsinki, P.O. Box 64, FIN-00014 Helsinki, Finland

(Received 22 November 2005; accepted 21 July 2006; published online 22 August 2006)

We determine the nucleation ability of argon clusters from Monte Carlo simulations. The nucleation rate appears to be defined by a sole characteristic of the clusters, namely, the stability. The stability is calculated as the ratio of grand canonical growth and decay rates and can be assigned to individual cluster configurations. We study the connection between the stability of the cluster configurations and their volume and total potential energy. Neither the potential energy nor the volume of a cluster configuration has a clear relation to its stability, and thus to the nucleation ability. On the other hand, we show that it is possible to use a specific volume for each cluster size to calculate the work of the cluster formation. These clusters with a unique volume have the same average stability as the full set of clusters. Our simulation method allows us to study the effect of possible deviations from equilibrium in the cluster configuration distributions. We argue that the nucleation process itself can produce a source for such a deviation. We show that even a small deviation from equilibrium in the cluster configuration distribution can lead to a dramatic deceleration of the nucleation rate. Although our simulations may overestimate the magnitude of the effect, they give qualitative estimates for its importance. © *2006 American Institute of Physics*. [DOI: 10.1063/1.2336776]

I. INTRODUCTION

The theoretics of nucleation is deeply related to the properties of nucleating clusters. The classical nucleation theory[1–3] (CNT) treats clusters as tiny bits of bulk material sharing the same thermodynamic properties. CNT successfully provides a simple and general theory of nucleation, but unfortunately its predictions for the nucleation rate are often unsatisfactory. In particular, the temperature dependency of the nucleation rate given by the theory is generally too strong compared to experiments.[4–6] The extensions[7–10] to CNT have not been able to make the agreement better. The self-consistent form[10] of CNT improves the temperature dependence of the theory, but fails to provide accurate predictions for the experimentally measured nucleation rates. Scaling models[6,11] based on CNT have also been proposed, and they successfully predict some of the experimental nucleation rates. However, we still lack a rigorous theory of nucleation that would explain the experimental results accurately.

Much attention has been focused to microscopic approaches based on molecular interactions. There are several efficient Monte Carlo methods[12–18] available for the calculation of the free energy of cluster formation, which is the key quantity required for the evaluation of nucleation rate. However, the classical molecular interaction models applied with the methods are always simplifications of the true interactions governed by complex quantum mechanical laws. Because of this, if two different model potentials are used in nucleation simulations of the same substance, one may observe large differences in evaluated nucleation rates. However, in case of homogeneous nucleation of water, the temperature dependence of the nucleation rate given by different potentials is in good agreement with experiments.[18] This is encouraging for the molecular approach to nucleation.

Two important assumptions in the present molecular nucleation theories are the equilibrium of the clusters and the inverse order of averaging for the calculation of the nucleation rate. The latter one implies that, instead of considering how individual droplets develop into the critical droplets and taking the average of those individual rates, theoreticians consider the rate at which an average cluster develops into the critical droplet. It is usually argued that the clusters quickly reach equilibrium after acquiring a molecule or evaporating one. In that case, the growth rate of a cluster is independent of the growth history of the cluster, and inverting the order of averaging is justified. The equilibrium of the clusters means that the probability to observe cluster configurations is proportional to the Boltzmann factor $\exp(-U_i/kT)$, where U_i is the internal cluster potential energy, k is the Boltzmann constant, and T is the temperature. In the literature the validity of the equilibrium of clusters has already been questioned.[19,20]

Further development of molecular approaches can be done with the inclusion of the nonaveraged cluster properties. To that end, the cluster definition which has the volume of the cluster as a parameter has been introduced.[19] In the dynamical nucleation theory the nucleation rate is calculated through the evaporation rate;[21] it allows one not to use the thermodynamic properties such as the free energy of the clusters, but to deal only with the kinetic variables.

In contrast to the molecular approach, the modified classical nucleation theories use only macroscopic parameters and need no intermolecular potentials. Recently developed extended modified liquid drop (EMLD) model appears to be

[a]Electronic mail: joonas.merikanto@helsinki.fi

compatible with molecular approaches.[22] Therefore, it is important to find a link between the parameters needed for liquid drop models and values provided by simulations.

For developing future nucleation theories, whether based on equilibrium assumption or not, it is important to understand how the differences between molecular configurations affect their nucleation ability. The current paper studies the stability properties of nucleating clusters with the aid of Monte Carlo simulations for argon. We show that each cluster configuration can be assigned with specific decay and growth probabilities. Their ratio describes the stability of the configuration, and hence its nucleation ability.

The method presented in this study is based on a Monte Carlo approach developed earlier.[18,23] It allows one to study the nucleation ability (the stability) of individual cluster configuration. The calculation of stability for a large number of cluster configurations, whose probability to exist is weighted according to allowed phase space, gives the stability distribution for the studied cluster size under given temperature and supersaturation. We study how the stability distribution evolves with the cluster size and how the stability is linked to intrinsic properties of the clusters such as their volume and potential energy. We locate the average clusters participating in nucleation, having unique volumes or potential energies but exhibiting the same work of formation behavior as the whole set of clusters.

We also illustrate the importance of understanding whether the clusters are in equilibrium or not. We demonstrate that even very small deviations of the clusters from equilibrium lead to dramatic changes of the nucleation rate.

II. THEORETICAL BACKGROUND TO THE SIMULATION METHOD

In our Monte Carlo method[18,23] we simulate one cluster at a time with a fixed number of particles. The cluster configuration space is traced out in a canonical Metropolis simulation. Instead of letting the cluster size fluctuate in a grand canonical fashion, we only calculate the probabilities for the grand canonical annihilation and creation moves. Earlier,[18,23] we have shown how the resulting average grand canonical cluster growth and decay probabilities can be linked to the kinetic condensation and evaporation rates of Becker and Döring.[2] Here, we give a short revision of the theoretical concepts behind the simulation technique.

We consider a cluster of n fully interacting cluster particles with $n_{\max}-n$ noninteracting particles at arbitrary positions inside a large simulation box of volume V, the center of mass of the cluster being placed at the center of the simulation box. The annihilation probability $A(n,\{\mathbf{R}_i\}\ominus\mathbf{R}_j)$ for an interacting cluster particle at a position $\mathbf{R}_j$ is given by

$$A(n,\{\mathbf{R}_i\}\ominus\mathbf{R}_j) = \frac{n}{\gamma VZ}\exp\left\{\frac{-[U_{n-1}(\{\mathbf{R}_i\}\ominus\mathbf{R}_j)-U_n(\{\mathbf{R}_i\})]}{kT}\right\}, \quad (1)$$

where $\gamma=1/\lambda^{-3}$, λ is the de Broglie wavelength of the particles, $U_n(\{\mathbf{R}_i\})$ is the total interaction energy associated with the configuration $\{\mathbf{R}_i\}$, k is the Boltzmann constant, and T is the temperature. The notation $\{\mathbf{R}_i\}\ominus\mathbf{R}_j$ indicates that the particle at position $\mathbf{R}_j$ is turned to noninteracting form configuration $\{\mathbf{R}_i\}$. The activity $Z=\exp[\mu/(kT)]$, where μ is the chemical potential, is equal to the number density of the surrounding vapor under the ideal gas assumption. The probability to turn a noninteracting particle into a fully interacting particle, the creation probability $C(n,\{\mathbf{R}_i\}\oplus\mathbf{R}_k)$, is given by

$$C(n,\{\mathbf{R}_i\}\oplus\mathbf{R}_k) = \frac{\gamma VZ}{n+1}\exp\left\{\frac{-[U_{n+1}(\{\mathbf{R}_i\}\oplus\mathbf{R}_k)-U_n(\{\mathbf{R}_i\})]}{kT}\right\}. \quad (2)$$

The probability of a certain n cluster to decay into an $(n-1)$ cluster during a Monte Carlo step is given by summing up the individual annihilation probabilities for each interacting cluster particle and normalizing the sum with the number of particles n,

$$D_n(\{\mathbf{R}_i\}) = \frac{\alpha_D}{n}\sum_{j=1}^{n}\delta_{\mathrm{clu}}\min[1,A(n,\{\mathbf{R}_i\}\ominus\mathbf{R}_j)], \quad (3)$$

where α_D is the probability that the annihilation is attempted during a Monte Carlo step and δ_{clu} is zero when annihilation would result in splitting the resulting $(n-1)$ cluster into two or more clusters according to given cluster definition, and 1 otherwise.

In a similar fashion, the probability of an n cluster to grow to an $(n+1)$ cluster during a Monte Carlo step is given by summing up the probabilities of the $n_{\max}-n$ possible noninteractive particle creations and normalizing with the number of attempts $n_{\max}-n$

$$G_n(\{\mathbf{R}_i\}) = \frac{\alpha_C}{n_{\max}-n}\sum_{k=1}^{n_{\max}-n}\delta_{\mathrm{clu}}\min[1,C(n,\{\mathbf{R}_i\}\oplus\mathbf{R}_k)]. \quad (4)$$

The creation is attempted during a Monte Carlo step with a probability $\alpha_C=\alpha_D$. δ_{clu} now ensures that the created particle becomes a part of the cluster according to the applied cluster definition.

During a simulation, $D(n,\{\mathbf{R}_i\})$ and $G(n,\{\mathbf{R}_i\})$ are calculated for a large number of configurations $\{\mathbf{R}_i\}$ created according to the Monte Carlo Metropolis scheme. They can be summed up and normalized with the number of configurations in order to gain the canonical ensemble averages of the growth and decay probabilities $\bar{G}_n$ and $\bar{D}_n$. This procedure is carried out for each cluster size n separately. Earlier,[18] we have shown that the detailed balance

$$P_n\bar{G}_n = P_{n+1}\bar{D}_{n+1}, \quad (5)$$

where P_n is the probability to observe an n cluster, holds. We also showed that the work of formation (also referred to as the Gibbs free energy) of an n cluster ΔW_n has a simple relation to the growth and decay probabilities $\bar{G}_n$ and $\bar{D}_n$

$$\Delta W_n = -kT\sum_{j=2}^{n}\ln\frac{\bar{G}_{j-1}}{\bar{D}_j}, \quad (6)$$

which has the same form as ΔW_n derived from the kinetic approach[2,24]

$$\Delta W_n = -kT\sum_{j=2}^{n} \ln \frac{\beta_{j-1}}{\alpha_j}, \tag{7}$$

where β_{n-1} is the condensation rate constant for an $(n-1)$ size cluster and α_n is the evaporation rate constant for an n-size cluster.

III. COMPUTATIONAL DETAILS

Our Monte Carlo method simulates isolated clusters of fixed size without explicitly involving the surrounding vapor. In this paper we have applied the method to simulations of argon clusters. The interaction between the argon atoms is described by the Lennard-Jones potential

$$\varphi_{ij}(R_{ij}) = 4\varepsilon\left\{\left(\frac{\sigma}{R_{ij}}\right)^{12} - \left(\frac{\sigma}{R_{ij}}\right)^{6}\right\}, \tag{8}$$

where R_{ij} is the distance between molecules i and j, and ε and σ are the energy and distance parameters of the selected potential, respectively. In our simulations we used the full potential without cutoff with parameters $\varepsilon=119.4$ K and $\sigma=3.4$ Å.

We have applied the Stillinger cluster definition,[25] stating that each molecule in a cluster must have another cluster molecule within some given connectivity distance, and that no molecules can exist within the connectivity distance that do not belong to the cluster. We have taken the connectivity distance to be 1.5σ, which is the standard choice for Lennard-Jones particles corresponding to the first minimum in the radial distribution function of liquid argon.

Simulations of argon nucleation have been carried out at 60 K temperature and with monomer vapor number densities $7.59\times10^{-4}\sigma^{-3}$ and $1.90\times10^{-3}\sigma^{-3}$ (corresponding to saturation ratios $S=20$ and $S=50$ assuming the simulated vapor behaves like ideal argon gas[26]). In a simulation, a single isolated cluster is placed on the center of a large spherical simulation box, and no periodic boundary conditions are applied. During the simulation, we assure that the center of mass of the cluster coincides with the center of the simulation box. The size of the simulation box does not affect the results as long as the selected simulation box is large enough, so that cluster particles are always far from the walls of the box. Randomly generated initial cluster configurations containing n argon atoms were first equilibrated for $n\times10^5$ Monte Carlo steps. Then, an additional 200×10^6 cluster configurations were created and one in thousand configurations was analyzed, totaling to 200 000 analyzed configurations that were significantly different from each other. The main values that are calculated were the growth and decay rates $G_n(\{\mathbf{R}_i\})$ and $D_n(\{\mathbf{R}_i\})$ given by Eqs. (4) and (3), the spherical cluster volume $V_n(\{\mathbf{R}_i\})$ with a radius defined as the distance of the furthest cluster particle from the center of mass of the cluster, and the total potential energy $U_n(\{\mathbf{R}_i\})$ for different cluster configurations $\{\mathbf{R}_i\}$.

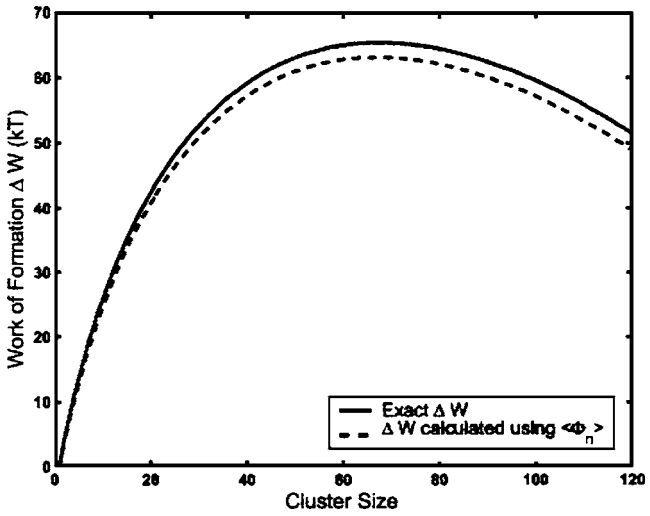

FIG. 1. Works of cluster formation for argon vapor at 60 K and $S=20$ calculated from Eqs. (6) (continuous line) and (11) (dashed line).

IV. APPLICATIONS OF THE METHOD

A. The stability of individual cluster configurations

If a cluster is characterized by the number of molecules only, its properties are thermal averages over all possible cluster configurations. Molecular simulations provide a means to study individual configurations and their contribution to the average values. We consider a similar cluster formation mechanism as in the kinetic nucleation theory by Becker and Döring. Nucleation is described as a chain of reactions

$$(1) + (n-1) \underset{\alpha_n}{\overset{\beta_{n-1}}{\rightleftharpoons}} (n). \tag{9}$$

Here, only condensation and evaporation of monomers are considered as they dominate in the nucleation process of nonassociating vapors.[27] As Eqs. (6) and (7) show, the averages of the grand canonical growth and decay probabilities $\bar{G}_n$ and $\bar{D}_n$ gained from the simulation can be related to condensation and evaporation rates β_n and α_n according to

$$\frac{\bar{G}_{n-1}}{\bar{D}_n} = \frac{\beta_{n-1}}{\alpha_n}. \tag{10}$$

Average values $\bar{G}_n$ and $\bar{D}_n$ are quite smooth functions of n. Hence, we can assume that Eq. (6) can be transformed to

$$\Delta W_n \simeq -kT\sum_{j=2}^{n} \ln \frac{\bar{G}_j}{\bar{D}_j}, \tag{11}$$

where we have replaced $\bar{G}_{j-1}$ in the numerator by $\bar{G}_j$.

We have carried out simulations of clusters containing between 1 and 120 argon atoms at temperature $T=60$ K and saturation ratio $S=20$. Our results shown in Fig. 1 verify that the difference between right hand sides of Eqs. (6) and (11) is small. At the critical cluster size the difference in ΔW does not exceed $1.5kT$. Thus, we can characterize each cluster size with the average instability

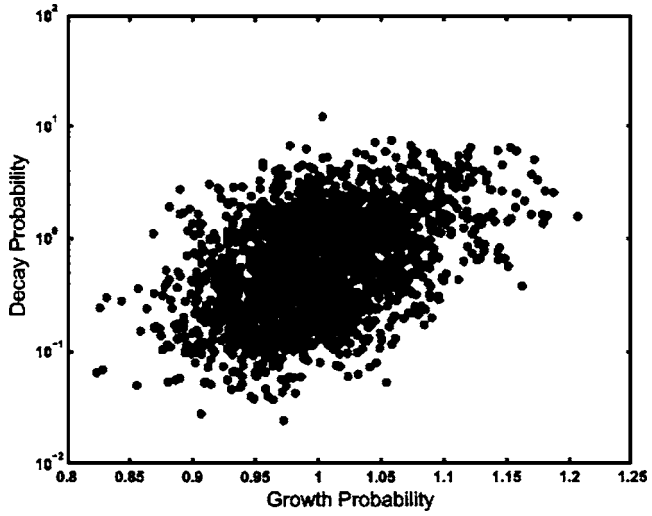

FIG. 2. Connection between the growth probability and the decay probability for an argon cluster at $T=60$ K and at $S=20$. The cluster contains 68 atoms and corresponds to the critical cluster. The probabilities have been scaled with respect to the average growth probability $\bar{G}_{68}=1$.

$$\langle \Phi_n \rangle = \frac{\bar{D}_n}{\bar{G}_n}. \tag{12}$$

If the average instability is less or more than 1, the cluster is overcritical or undercritical, respectively. For the critical cluster size n^*, the instability is $\langle \Phi_{n^*} \rangle = 1$. We also define the cluster stability as the inverse value of the instability.

The variations in $G_n(\{\mathbf{R}_i\})$ and $D_n(\{\mathbf{R}_i\})$ between different cluster configurations $(\{\mathbf{R}_i\})$ are shown in Fig. 2 for $n=68$ representing the critical cluster. Note that the y axis representing the decay probability in the figure is logarithmic, while the x axis representing the growth probability is linear. The figure shows that $G_n(\{\mathbf{R}_i\})$ and $D_n(\{\mathbf{R}_i\})$ are slightly correlated, and that the variation in $D_n(\{\mathbf{R}_i\})$ is more than two orders of magnitude between different cluster configurations, whereas variations in $G_n(\{\mathbf{R}_i\})$ are within 40%. An enhanced growth probability of a cluster is greatly overcompensated by the enhanced decay probability.

Since the growth probability varies only little between different cluster configurations, we can express the ratio between mean growth and decay probabilities of an n-size cluster approximately as

$$\frac{\bar{D}_n}{\bar{G}_n} = \frac{D_n(\{\mathbf{R}_i\}) + D_n(\{\mathbf{R}_j\}) + \cdots + D_n(\{\mathbf{R}_l\})}{G_n(\{\mathbf{R}_i\}) + G_n(\{\mathbf{R}_j\}) + \cdots + G_n(\{\mathbf{R}_l\})} \approx \frac{1}{l}\left[\frac{D_n(\{\mathbf{R}_i\})}{G_n(\{\mathbf{R}_i\})} + \frac{D_n(\{\mathbf{R}_j\})}{G_n(\{\mathbf{R}_j\})} + \cdots + \frac{D_n(\{\mathbf{R}_l\})}{G_n(\{\mathbf{R}_l\})}\right], \tag{13}$$

where l represents the total number of studied configurations and the subscripts $i,j,\ldots,l$ correspond to the different cluster configurations. The difference between the right hand side and the left hand side of Eq. (13) turns out to be 3% at most. This fact is not trivial because the variation in denominators in the right hand side is about 40%, while the sum of ratios gives only 3% difference from the exact value. It is evidently a consequence of the correlation of the growth and decay rates shown in Fig. 2.

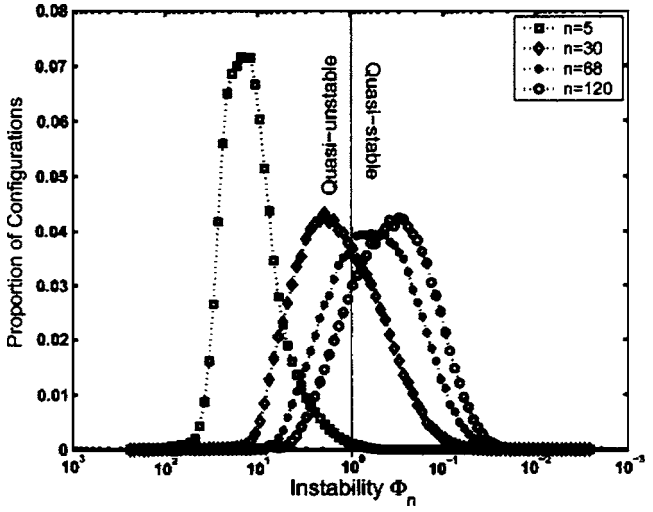

FIG. 3. Distribution of instability Φ_n for $n=5$, 30, 68, and 120 from left to right. $\Phi_n=1$ is shown with a vertical line. Simulations were carried out for argon at $T=60$ K and $S=20$.

Results (13) allows us to assign instability $\Phi_n(\{\mathbf{R}_i\})$ to each individual cluster configuration $\{\mathbf{R}_i\}$:

$$\Phi_n(\{\mathbf{R}_i\}) = \frac{D_n(\{\mathbf{R}_i\})}{G_n(\{\mathbf{R}_i\})}. \tag{14}$$

If $\Phi_n(\{\mathbf{R}_i\}) < 1$, the probability that the configuration $(\{\mathbf{R}_i\})$ grows to size $n+1$ is greater than the probability of $(\{\mathbf{R}_i\})$ decaying to size $n-1$. We call these configurations the quasistable configurations. Figure 3 shows the instability distribution for the clusters containing 5, 30, 68, and 120 atoms. $\bar{D}_n/\bar{G}_n$ is 15.38, 2.26, 0.99, and 0.61 for these cluster sizes, respectively. On a logarithmic scale the instability distribution has a form of a skewed Gaussian distribution. The variation of instability between different cluster configurations is significant both for small and large clusters.

The total proportion of quasistable configurations as a function of cluster size is presented in Fig. 4. The work of cluster formation calculated from Eq. (6) is also shown. The

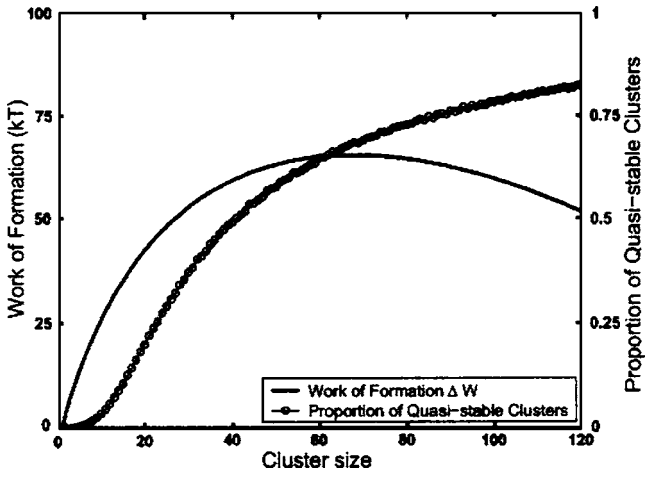

FIG. 4. Work of cluster formation for argon at $T=60$ K and $S=20$ and the corresponding proportion of quasistable configurations as functions of cluster size. The critical cluster contains 68 argon atoms and has 68% of quasistable configurations.

figure illustrates that even clusters containing only a few argon atoms have configurations that are quasistable. For the critical cluster containing 68 atoms, 68% of the configurations are quasistable. Clusters containing a large number of atoms compared to the critical size still have a large proportion of configurations that decay more easily than grow.

At first sight it seems that for the critical cluster the proportion of the quasistable clusters should be 50%. However, careful consideration shows that it is not necessarily so. Indeed, for the critical cluster the net growth flux is exactly compensated for by the net decay flux. The balance requirement can be written as

$$\sum_i [G_{n^*}(\{\mathbf{R}_i\}) - D_{n^*}(\{\mathbf{R}_i\})]P_{n^*}(\{\mathbf{R}_i\}) = \sum_j [D_{n^*}(\{\mathbf{R}_j\}) - G_{n^*}(\{\mathbf{R}_j\})]P_{n^*}(\{\mathbf{R}_j\}), \quad (15)$$

where index i counts over quasistable configurations and j counts over quasiunstable configurations. From Eq. (15) one should not expect $\Sigma_i P_{n^*}(\{\mathbf{R}_i\})=0.5$ or $\Sigma_j P_{n^*}(\{\mathbf{R}_j\})=0.5$.

Equations (11), (13), and (14) show us that the work of the cluster formation can be calculated by using instabilities of individual cluster configurations. A configuration with lower instability contributes to the nucleation rate

$$I \propto \exp\left(-\frac{\Delta W_{n^*}}{kT}\right) \approx \frac{1}{\Pi_{j=2}^{n^*}\left[(1/l)\Sigma_{i=1}^{l}\Phi_j(\{\mathbf{R}_i\})\right]} \quad (16)$$

more significantly than one with higher instability.

However, we note that the above expression does not describe the true dynamics of clusters. Importantly, the quasistable configurations can create an unstable configuration by acquiring or evaporating a monomer, and vice versa. Thus, we may not argue that only quasistable clusters contribute to nucleation. Furthermore, summation over quasistable clusters alone would lead to incorrect results; the forward rate and backward rate contributions must all be taken into account. Also, we have only considered clusters described with the equilibrium configuration distribution. Thus, we have neglected the relaxation process of new-born clusters, and presumed a rate theory which only takes into account the growth and decay of equilibrated clusters.

What Eqs. (11), (13), and (14) can do is to determine the contribution of each cluster configuration to the nucleation process. Thus, for a snapshot of cluster configurations taken at any time, we can clearly show which configurations add weight to the nucleation rate more than others. Importantly, we have found a characteristic value which defines the nucleation ability of each individual configuration. It is also vital that this characteristic value can be calculated with Monte Carlo simulations. One can apply calculations of the cluster stabilities to determine the characteristics of average clusters contributing to nucleation, as we do in Sec. IV C. Besides that, it seems that for the equilibrium molecular theory the knowledge of the nucleation ability of cluster configurations does not offer other direct applications. However, for the molecular approach which takes into account the deviations from the equilibrium cluster configuration distribution, this knowledge might be important. If we know the nonequilibrium cluster configuration distribution for each cluster size, we are able to calculate the work of cluster formation using values of the cluster configuration instabilities defined by Eq. (14).

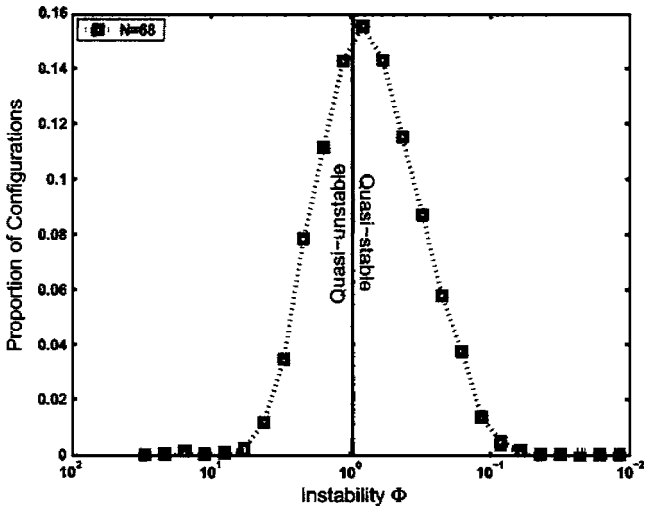

FIG. 5. Distribution of instability Φ_n for $n=68$ calculated for a single volume bin corresponding to volume with average instability $V_{\langle\Phi\rangle}$. $\Phi_n=1$ is shown with a vertical line. The width of the instability distribution is only slightly narrower than the width of the instability distribution for all volumes shown in Fig. 3.

B. Growth and decay probabilities with respect to intrinsic cluster properties

We now study the relationship between the cluster instability and its volume V and total potential energy U. For the calculation of V we define the radius of the cluster by calculating the distance of the furthest cluster molecule, the "shell molecule," from the center of mass of the cluster. Using this definition of cluster volume together with the Stillinger cluster definition, we actually obtain the n/v Stillinger cluster, which is the centerpiece of a molecular nucleation model of Senger *et al.*[19]

We study the critical cluster size $n^*=68$ in detail. Figure 3 shows the instability distribution for this size calculated from all configurations. We organize the simulation results in narrow energy and volume bins, and calculate the average growth and decay probabilities as well as the average instability corresponding to each bin. Figure 5 illustrates the instability distribution for the critical cluster restricted to a single volume. The selected volume corresponds to that of the average cluster participating in nucleation, a concept further explained in the next subsection. We observe the instability distribution to be as wide as the distribution for all configurations shown in Fig. 3. Figure 6 demonstrates the moderate connection between the instability of the cluster and its volume. There is some correlation between the volume of configuration and its stability, the correlation coefficient being 0.62. Similar results were observed also when comparing potential energy with stability. Therefore, neither the cluster volume nor the energy can be used to characterize the nucleation ability of the cluster configurations.

Figure 7 shows the growth and decay probabilities as well as the instability for the critical cluster as a function of

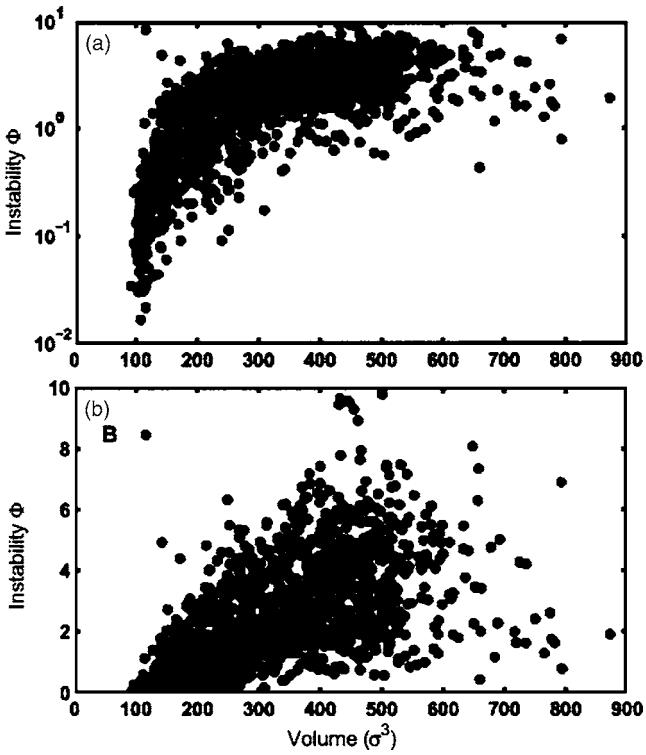

FIG. 6. Instability Φ_n vs volume for $n=68$ cluster. In (A), Φ_n is shown on a logarithmic scale to emphasize the variation in Φ_n with respect to all volume states. In (B), Φ_n is shown on a linear scale to emphasize the slight correlation between Φ_n and volume.

the cluster volume. The growth probability of clusters increases only slightly with increasing cluster volume. This is due to only a moderate increase in the available volume where new cluster particles can be added to satisfy the Stillinger cluster definition, and due to subsequent weakening of the cluster potential energy. The decay probability, however, is a strong function of the cluster volume. Thus, the variation in cluster instability is almost entirely associated with the variation in decay probability. The most stable states of the cluster correspond to the smallest cluster volumes, and larger

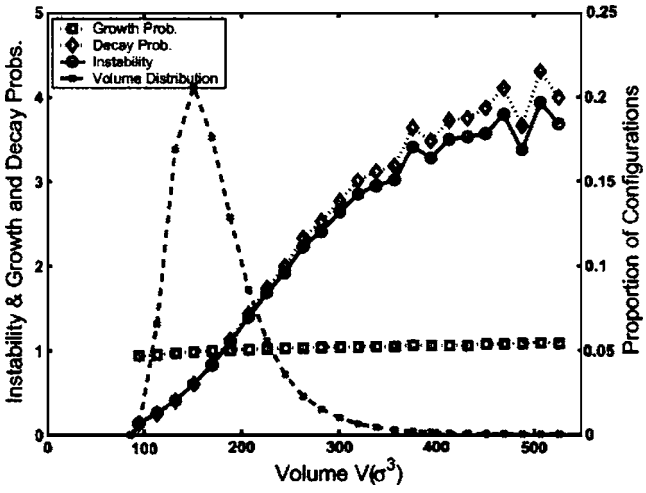

FIG. 7. Instability Φ, growth probability, and decay probability for the critical cluster $n^*=68$ as functions of cluster volume V on the left y axis. The distribution of cluster volume during the simulation is shown on right y axis as a proportion of all configurations.

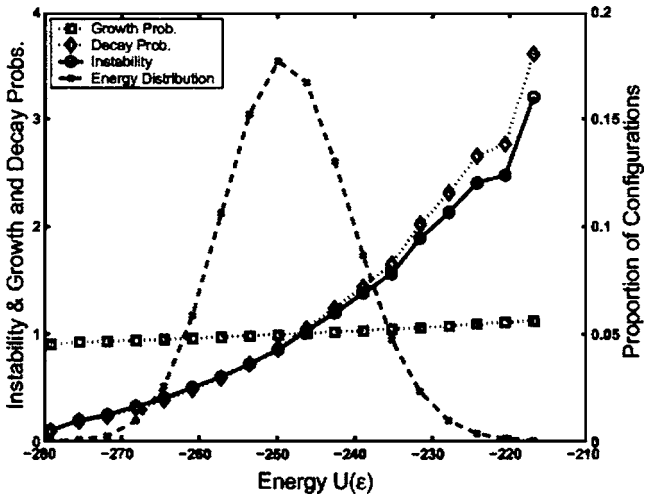

FIG. 8. Instability Φ, growth probability, and decay probability for the critical cluster $n^*=68$ as functions of the total cluster potential energy U on the left y axis. The distribution of the total potential energy during the simulation is shown on the right y axis as a proportion of all configurations.

clusters tend to evaporate more easily. The proportion of quasistable states according to the volume distribution for the critical cluster is 62% compared to 68% proportion, all states being quasistable. The difference arises from the averaging of growth and decay probabilities for each volume state; while most of the cluster configurations can be stable for a given cluster volume making it stable on average, there can still exist some configurations that decay more easily than grow. Figure 8 shows the variation of growth and decay probabilities as well as the instability as a function of cluster interaction energy. The variations in the cluster growth and decay probabilities are similar to the ones shown in the previous figure. The proportion of quasistable states according to the energy distribution is again 62%. We have thus demonstrated that sorting the cluster configurations by the value of their volume or energy does not enable us to calculate the number of quasicritical configurations. This is a consequence of only a moderate correlation between the stability and volume or energy.

C. The average cluster participating in nucleation

Most molecular nucleation theories are based on the assumption of cluster equilibrium. Therefore, all of them lead to the expression of nucleation rate which look like Eq. (16). Different theories differ in the way a cluster is defined and in the method of calculating ΔW_{n^*}. If the same cluster definition and molecular interaction model are used all methods should give the same results, provided that the same equilibrium principles are used both for the internal structure of the clusters and for the cluster size distribution. When calculating ΔW_{n^*} in molecular theories, all possible cluster configurations are taken into account. In contrast, in the classical theory and its modifications, droplets of each size are assumed to have only one volume. Clearly, the molecular approach is more rigorous, but the classical theory has the advantage of being able to assign macroscopic properties to the droplet. That is why the attempts to find an average nucleating cluster, whose properties can be related to a macroscopic

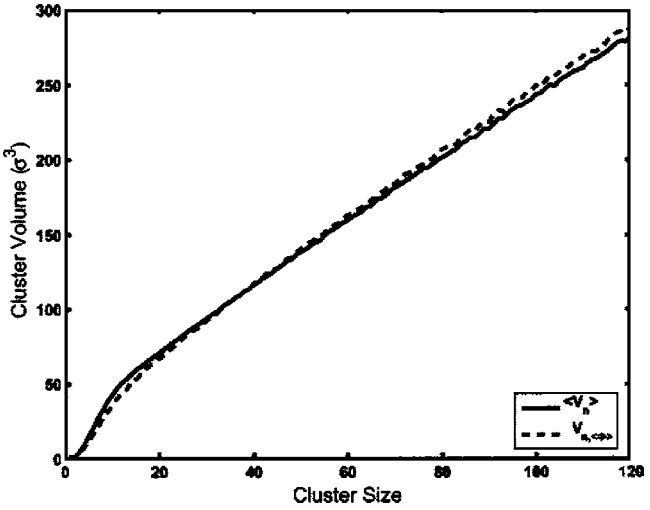

FIG. 9. Average volume $\langle V \rangle$ of clusters and the volume corresponding to average instability $V_{\langle \Phi \rangle}$ shown as functions of cluster size.

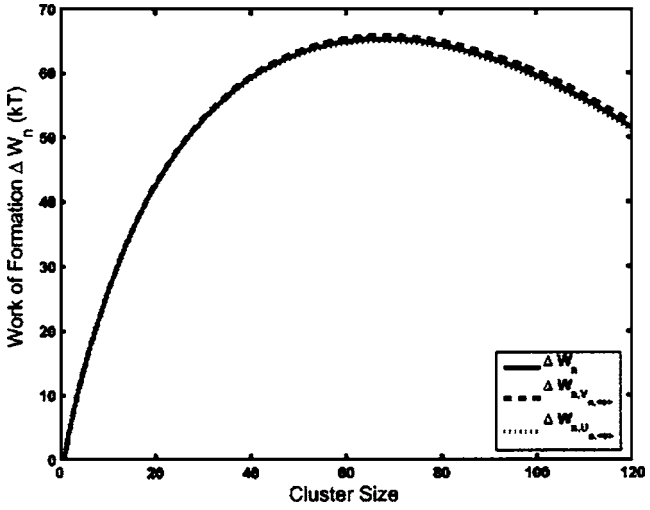

FIG. 10. Work of formation of all cluster ΔW_n, clusters having volume corresponding to average instability $\Delta W_{n,V_\Phi}$, and clusters having potential energy corresponding to average instability $\Delta W_{n,U_\Phi}$ shown as functions of cluster size.

droplet, are still going on. The average cluster is the cluster of certain volume or energy which gives the same ΔW_n as the whole spectrum of clusters of the same size. In attempts to improve the classical nucleation theory, several liquid drop models have been used to describe the clusters participating in nucleation.[7,9,22,28] In recent EMLD model[22] the volume of the droplet is calculated by minimizing either the change of free energy or the evaporation flux from the droplet[21] with respect to volume. These two cases proved to be equivalent.[22]

To verify EMLD model from the microscopic point of view, we have looked for the average cluster participating in nucleation. This n-size cluster has the same nucleation ability as the whole set of n-size clusters with varying characteristic properties such as volumes or potential energies, but with one characteristic property fixed. Thus, this cluster is defined both according to the number of molecules it contains and an additional condition, which in here is taken to be either its volume V or its potential energy U. We showed in Sec. IV A that one can express the work of cluster formation through the stability of clusters. Now, we locate the volumes and potential energies of the configurations for which the instability is, on average, the same as for the whole set. The volume $V_{n,\langle \Phi \rangle}$, for which the average instability of the n-size cluster corresponds to the average instability $\langle \Phi \rangle$ over all configurations, is displayed in Fig. 9 as a function of cluster size. We see that $V_{n,\langle \Phi \rangle}$ follows the average volume $\langle V_n \rangle$ fairly closely, but has a slightly different slope as a function of cluster size compared to $\langle V_n \rangle$. At small cluster sizes $V_{n,\langle \Phi \rangle}$ is less than $\langle V_n \rangle$, and at larger sizes $V_{n,\langle \Phi \rangle}$ exceeds $\langle V_n \rangle$. When a similar analysis is carried out for potential energies, it turns out that $U_{n,\langle \Phi \rangle}$ is ~ 0.17 standard deviations higher than $\langle U_n \rangle$ for all clusters, corresponding to less confined potential energy states. This difference is only about one-fourth of the difference in average potential energies of n and $n+1$ clusters.

We calculate the work of cluster formation W_{n,V_n} corresponding to a selected volume or potential energy bin. The works or formation of such clusters are described by expressions

$$\Delta W_{n,V_n} = -kT \sum_{j=2}^{n} \ln \frac{\bar{G}_{j-1,V_{j-1}}}{\bar{D}_{j,V_j}}, \tag{17}$$

$$\Delta W_{n,U_n} = -kT \sum_{j=2}^{n} \ln \frac{\bar{G}_{j-1,U_{j-1}}}{\bar{D}_{j,U_j}}, \tag{18}$$

where $\bar{G}_{n,V_n}$ and $\bar{D}_{n,V_n}$ are the average growth and decay probabilities of n-size clusters having volumes V_n, and $\bar{G}_{n,U_n}$ and $\bar{D}_{n,U_n}$ are the corresponding probabilities of clusters having potential energies U_n. Calculations of the work of formation of $V_{\langle \Phi \rangle}$ and $U_{\langle \Phi \rangle}$ clusters using Eqs. (17) and (18) show that these clusters indeed yield the ΔW_n behavior equal to the whole set of clusters with varying volumes and potential energies. This is illustrated in Fig. 10, which demonstrates that all three work of formation curves lie on top of each other. Furthermore, we have checked that clusters chosen according to some other criteria than the average instability do not produce the correct work of formation curve. Thus, we have identified the average nucleation pathway of Stillinger clusters as a function of cluster volume and potential energy. We have proven that it is possible to choose one specific volume for each cluster size in order to correctly describe the work of the cluster formation, and hence the nucleation rate. This supports the idea behind the EMLD model.

D. Nucleation in a perturbed system

In the the Becker-Döring approach the steady state nucleation rate is defined through the following set of kinetic equations:

$$\frac{\partial N_n}{\partial t} = \beta_{n-1}N_{n-1} + \alpha_{n+1}N_{n+1} - \beta_n N_n - \alpha_n N_n, \tag{19}$$

where N_n is the concentration of clusters containing n molecules, β_n is the condensation rate of monomers onto a cluster, and α_n is the evaporation rate from the cluster. Defining net rate I_n as

$$I_n = \beta_n N_n - \alpha_{n+1}N_{n+1}, \tag{20}$$

we can write Eq. (19) as

$$\frac{\partial N_n}{\partial t} = I_{n-1} - I_n. \tag{21}$$

Two time-independent cases are considered. The first is the balanced steady state where the net rate is zero, $I_n=0$, for all sizes n, and thus we observe the detailed balance

$$\beta_n N_n = \alpha_{n+1}N_{n+1}. \tag{22}$$

From the thermodynamic point of view, the balanced steady state is considered as the metastable equilibrium with the equilibrium distribution for sizes and configurations. The second case is the unbalanced steady state where the net rate I_n is independent of n but not zero and is equal to the nucleation rate. In both cases the left hand side of Eq. (21) is zero and N_n is thus time independent, but the steady state cluster distributions are different. The cluster work of formation is calculated in the balanced steady state, and the unbalanced state only affect the preexponent factor in Eq. (16) for the nucleation rate. This is the standard routine for calculating the nucleation rate.[29,30]

However, it is not self-evident that nucleation can be described by calculating the condensation and evaporation rates for the equilibrium cluster configuration distribution.[19,20] Indeed, the nucleation process itself can change this distribution, Evaporation and condensation events occur at some specific locations of the clusters, which define the boundary of the clusters. The portion of the particles that are situated at these boundary states define the cluster evaporation rate. Since the net flux I_n in the nucleating vapor is positive, the statistical weight of cluster configurations with a high number of boundary particles can be higher than in the case of equilibrated distribution. Therefore, the average evaporation rate for the same size cluster can be higher in the nucleating vapor than in true equilibrium. The scale of this effect is unclear because, evidently, the cluster relaxation attenuates this effect. The average cluster relaxation time after acquisition of the molecule[31] is not very much shorter than the average cluster lifetime[32,33] and the average evaporation rate of the cluster population right after accommodation of a molecule is slightly higher than in the population of relaxed clusters. These facts indicate that the cluster configuration distribution in the nucleating vapor is slightly different from the one in the equilibrium vapor. However, even a small shift in this distribution can produce a strong effect on the nucleation rate.

Earlier,[18] we have established a link between the evaporation and condensation rates and the grand canonical growth and decay rates [see Eqs. (6), (7), and (10)]. In the derivation, the equilibrium of cluster distribution was a secondary issue, so we can conclude that similar relations are valid if the clusters do not follow the equilibrium distribution. These relations demonstrate a general isomorphism between a real nucleation process and imaginary grand canonical growth and decay moves. Therefore, by simulating the growth and decay of clusters with small deviations from the equilibrium configuration distribution, we can estimate the nucleation rate of nonequilibrium clusters.

We have performed simulations in a perturbed system to estimate how much the cluster configuration distribution in the nucleating vapor differs from the equilibrium distribution, and how this difference can affect the nucleation rate. The unperturbed distribution, corresponding to the equilibrium configuration distribution of n clusters, is represented by a distribution function $f_n(\{\mathbf{R}_i\})$ over which, in fact, we perform canonical averaging. For example, the growth rate is given by

$$\bar{G}_n = \int_V \prod_{i=1}^{n} d\mathbf{R}_i f_n(\{\mathbf{R}_i\}) G(n,\{\mathbf{R}_i\}), \tag{23}$$

where f_n is normalized to unity. Suppose that we pick only those configurations which occur just after creation or annihilation moves. The chosen distribution of configurations is clearly not the same as in equilibrium. On the other hand, deviation from the equilibrium distribution should not be big since the acceptance of acts of creation and annihilation are weighted according to the Boltzmann factor. Note that in real nucleating vapor, molecules arrive at the boundary states of a cluster, while in our Monte Carlo growth process, molecules can be placed at any available location (even at the center) in the cluster, and the growth moves are accepted according to the Boltzmann factor. It means that a configuration after a growth event does not correspond to a cluster state right after an arrival of a new molecule in the real nucleation process. It rather corresponds to a cluster state after partial relaxation; partial because the full thermalization or relaxation would involve also the restructuring of the body of the old cluster.

In Fig. 11 we have plotted the volume distribution for $n=70$ clusters born in creation events. We observe a small shift to higher volumes compared to the equilibrium cluster volume distribution. For smaller clusters the relative shift is slightly larger. The figure also demonstrates that the volume of clusters born in annihilation events practically follow the equilibrium volume distribution. As a consequence, the population of clusters born in creation events have, on average, a higher decay rate than the one calculated for the equilibrium cluster population. The average decay rate in a population of clusters born in annihilation events is almost the same as in equilibrium.

At first sight our simulated configuration distribution seems equivalent to the one obtained in the special case of grand canonical Monte Carlo, in which only the growth and decay moves are performed, but in fact there is a substantial difference. If the creation or annihilation move appears to be unsuccessful in the grand canonical Monte Carlo sampling, the old configurations is taken into account again. Thus the old configuration gains some more statistical weight. An infinite run of the grand canonical Monte Carlo sampling,

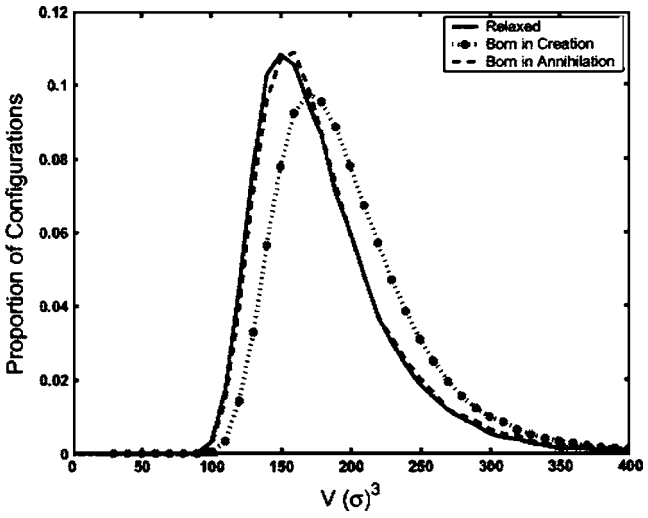

FIG. 11. Volume distributions of clusters containing 70 atoms. Continuous line corresponds to an equilibrium cluster distribution, dashed line to clusters born when one particle is annihilated from $n=71$ clusters, and dotted line to clusters born when one particle is created to $n=69$ clusters.

where canonical moves are not performed, should produce merely the equilibrium distribution. In our simulated distribution there are no unsuccessful creation or annihilation moves to give the additional statistical weight to the old configuration. Their contribution to the new distribution is just weighted according to their relative probability. This causes the expected shift from equilibrium, and we observe that our simulation gives a rather smooth distribution of volumes different from the equilibrium one. The smoothness convinces us that the sampled set is big enough.

Figure 11 demonstrates that the distribution of configurations just after the occurrence of creation or annihilation events imitates a small perturbation from the equilibrium distribution. The direction of the shift of the cluster configuration distribution is similar to the shift likely caused by nucleation. The magnitude of the shift is small and we use it as an estimate for the shift in the real nucleating vapor. Our aim is to demonstrate that even such a small shift can produce a strong effect on the nucleation rate, and thus attract more attention to the study of the cluster configuration distribution in the real nucleating vapor.

To calculate the work of formation for a perturbed system we need to average the growth and decay rates over the perturbed configuration distribution and then apply Eq. (6). The perturbed configuration distribution can be described by the distribution function $f_{n,p}(\{\mathbf{R}_i\})$ normalized to unity,

$$f_{n,p}(\{\mathbf{R}_i\}) = c_n f_{n,c}(\{\mathbf{R}_i\}) + a_n f_{n,a}(\{\mathbf{R}_i\}), \tag{24}$$

where $f_{n,c}(\{\mathbf{R}_i\})$ and $f_{n,a}(\{\mathbf{R}_i\})$ are the distribution function normalized to unity for clusters born after creation and annihilation, respectively, and c_n and a_n are the weights of the distribution functions. Figure 11 shows that $f_{n,a}(\{\mathbf{R}_i\})$ is very close to the equilibrium distribution function. From hereafter subscript p corresponds to a perturbed system or averaging over a perturbed distribution function, and subscripts c and a correspond to distribution functions of clusters born after creation and annihilation, respectively, or averaging over these functions. Since the distribution functions are normalized to unity, integration of Eq. (24) over all coordinates leads to

$$c_n + a_n = 1. \tag{25}$$

The number of n clusters born in annihilation events is defined by the decay rate of $(n+1)$ clusters, while the number of n clusters born in creation events is defined by the growth rate of $(n-1)$ clusters. Thus, the following equation holds:

$$\frac{c_n}{a_n} = \frac{P_{n-1,p}\bar{G}_{n-1,p}}{P_{n+1,p}\bar{D}_{n+1,p}}. \tag{26}$$

To calculate the work of formation of clusters in the perturbed system, we have to resort to the concept of corresponding balanced steady state; this is a state where the cluster size distribution has equilibrated, but the cluster configuration distribution is perturbed from the equilibrium. In the standard calculation of the nucleation rate the work of formation is solved from the detailed balance, which in turn is the solution of the balanced steady state case. The balanced steady state is an artificial construction, and imaginary constraints are needed to maintain it; this is also true in the case of the metastable equilibrium in a supersaturated vapor related to Eq. (22). All the consequences of the unbalanced steady state contribute to the preexponential factor, decreasing the nucleation rate by one or two orders of magnitude. We use the same approach, and construct the artificial balanced steady state for the nonequilibrated clusters. The consequences of the unbalanced steady state are again taken into account in the preexponential factor, which is of the same order as in the case of equilibrated clusters since the kinetic equations are formally the same in both cases. Thus, we may apply the detailed balance

$$P_{n,p}\bar{G}_{n,p} = P_{n+1,p}\bar{D}_{n+1,p} \tag{27}$$

also in the case of nonequilibrated clusters.

Using Eqs. (25)–(27), we obtain

$$c_n = \frac{\bar{D}_{n,p}}{\bar{D}_{n,p} + \bar{G}_{n,p}} \tag{28}$$

and

$$a_n = \frac{\bar{G}_{n,p}}{\bar{D}_{n,p} + \bar{G}_{n,p}}. \tag{29}$$

Equations (28) and (29) give us an explicit expression for the distribution function defined by Eq. (24), which allows us to average the growth and decay rates over the perturbed configuration distribution, producing

$$\bar{D}_{n,p} = \frac{\bar{D}_{n,p}}{\bar{D}_{n,p} + \bar{G}_{n,p}}\bar{D}_{n,c} + \frac{\bar{G}_{n,p}}{\bar{D}_{n,p} + \bar{G}_{n,p}}\bar{D}_{n,a} \tag{30}$$

and

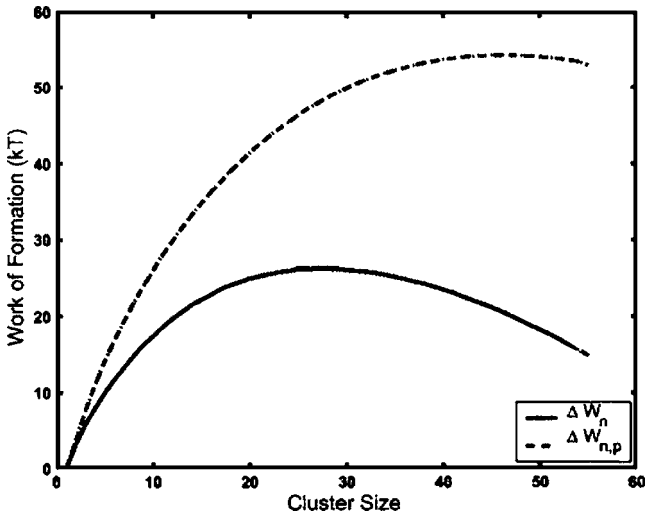

FIG. 12. Works of cluster formation ΔW_n (unperturbed configurations) and $\Delta W_{n,p}$ (perturbed configurations) from a simulation at $T=60$ K and $S=50$.

$$\bar{G}_{n,p} = \frac{\bar{D}_{n,p}}{\bar{D}_{n,p}+\bar{G}_{n,p}}\bar{G}_{n,c} + \frac{\bar{G}_{n,p}}{\bar{D}_{n,p}+\bar{G}_{n,p}}\bar{G}_{n,a}. \quad (31)$$

Values of $\bar{G}_{n,c}$ and $\bar{G}_{n,a}$ can be obtained via simulations, thus allowing us to find values for $\bar{D}_{n,p}$ and $\bar{G}_{n,p}$. We loosely use the growth and decay rates given by Eqs. (30) and (31) to estimate the work of formation in the perturbed system using Eq. (6). A sound proof of the relation between the work of formation and quantities $\bar{P}_{n,p}$, $\bar{D}_{n,p}$, and $\bar{G}_{n,p}$ related to the noncanonical distribution in the perturbed system is beyond the scope of this paper.

We carried out a simulation at 60 K and saturation ratio $S=50$. We calculated the work of cluster formation for the unperturbed system according to Eq. (6), and for the perturbed system by using values of $\bar{G}_{n,c}$ and $\bar{G}_{n,a}$ obtained with Eqs. (30) and (31). Figure 12 shows the resulting work of formation curves in the two cases. A huge increase in the work of formation can be seen if the system is perturbed. The energy barrier separating the two phases rises from $26.3kT$ to $54.3kT$, and the critical cluster size from $n^*=27$ to $n^*=46$. This would cause the nucleation rate to be suppressed by over 13 orders of magnitude.

Our result underlines the extreme sensitivity of the nucleation process; a small shift from equilibrium cluster configuration distribution leads to a dramatic change in the nucleation rate. The evaporation rate increases due to small perturbations in the cluster configuration distribution. Although the perturbations can be overestimated with the method we used, the effect is so large that even if the realistic perturbations are significantly smaller, they can still drastically suppress the nucleation rate. We believe that the result presented here gives a strong motivation to reconsider the theoretical framework behind equality of the evaporation rates for nucleating clusters and clusters in equilibrium.

V. SUMMARY

We have applied an earlier developed Monte Carlo method[18,23] to study properties of the individual cluster configurations in nucleating vapor. We have established that the work of the cluster formation is with a good accuracy defined by a sole characteristic, which can be assigned to individual cluster configurations. This characteristic is the stability of the cluster configurations. Therefore, the stability of a cluster configuration defines its nucleation ability. The stability has only a moderate correlation with the cluster volume and potential energy.

We have shown that it is possible to use one specific volume for each cluster size to calculate the work of cluster formation. For this cluster with a unique volume the average stability is equal to the average stability of all clusters. The EMLD model[22] does not require intermolecular potentials, but uses only macroscopic parameters. Therefore, it requires also the value of volume of the droplets. Our simulations have justified that such volume can be defined from the point of view of the molecular approach. A comparison between the volumes calculated with a macroscopic approach and molecular simulations is beyond the scope of this paper, but should be performed in the future.

The formalism that we have developed here and in our earlier works[18,23] allows us to calculate nucleation rate not only for the clusters in equilibrium, but also for nonequilibrium clusters. We have generated the cluster configuration distribution that differs slightly from the equilibrium distribution. The direction of the shift from equilibrium is the same as could be expected in a nucleating vapor, although our method probably overestimates the shift. We have shown that even small deviations from equilibrium in the cluster configuration distribution can lead to a dramatic deceleration of the nucleation rate. The assumption that the evaporation properties of nucleating clusters can be considered the same as those of equilibrium clusters should be carefully reconsidered.

[1] M. Volmer and A. Weber, Z. Phys. Chem., Stoechiom. Verwandtschaftsl. **119**, 277 (1925).
[2] R. Becker and W. Döring, Ann. Phys. **24**, 719 (1935).
[3] J. Zeldovich, Zh. Eksp. Teor. Fiz. **12**, 525 (1942).
[4] C. Hung, M. J. Krasnopoler, and J. L. Katz, J. Chem. Phys. **90**, 1856 (1989).
[5] R. Strey, T. Schmelling, and P. E. Wagner, J. Chem. Phys. **85**, 6192 (1986).
[6] J. Wölk and R. Strey, J. Phys. Chem. B **105**, 11683 (2001).
[7] J. Lothe and G. M. Pound, J. Chem. Phys. **36**, 2080 (1962).
[8] D. W. Oxtoby and R. Evans, J. Chem. Phys. **89**, 7521 (1988).
[9] A. Dillmann and G. E. A. Meier, J. Chem. Phys. **94**, 3872 (1991).
[10] S. L. Girshick and C.-P. Chiu, J. Chem. Phys. **93**, 1273 (1990).
[11] B. Hale, J. Chem. Phys. **122**, 204509 (2005).
[12] J. K. Lee, J. A. Barker, and F. F. Abraham, J. Chem. Phys. **61**, 1221 (1974).
[13] B. N. Hale and R. Ward, J. Stat. Phys. **28**, 487 (1982).
[14] P. R. ten Wolde and D. Frenkel, J. Chem. Phys. **109**, 9901 (1998).
[15] K. Oh and X. Zeng, J. Chem. Phys. **110**, 4471 (1999).
[16] I. Kusaka and D. Oxtoby, J. Chem. Phys. **113**, 10100 (2000).
[17] B. Chen, J. I. Siepmann, K. J. Oh, and M. L. Klein, J. Chem. Phys. **115**, 10903 (2001).
[18] J. Merikanto, H. Vehkamäki, and E. Zapadinsky, J. Chem. Phys. **121**, 914 (2004).
[19] B. Senger, P. Schaaf, D. S. Corti, R. Bowles, J.-C. Voegel, and H. Reiss, J. Chem. Phys. **110**, 6421 (1999).

[20] A. A. Lushnikov and M. Kulmala, Phys. Rev. E **58**, 3157 (1998).
[21] G. K. Schenter, S. M. Kathmann, and B. C. Garrett, Phys. Rev. Lett. **82**, 3484 (1999).
[22] D. Reguera and H. Reiss, Phys. Rev. Lett. **93**, 165701 1 (2004).
[23] H. Vehkamäki and I. J. Ford, J. Chem. Phys. **112**, 4193 (2000).
[24] D. Kashchiev, *Nucleation: Basic Theory with Applications* (Butterworth-Heinemann, Oxford, 2000).
[25] F. H. Stillinger, J. Chem. Phys. **38**, 1486 (1963).
[26] *CRC Handbook of Chemistry and Physics*, 83rd ed., edited by D. R. Lide (CRC, Boca Raton, FL, 2002).
[27] J. H. Seinfeld and S. N. Pandis, *Atmospheric Chemistry and Physics: From Air Pollution to Climate Change* (Wiley, New York, 1998).
[28] H. Reiss, W. K. Kegel, and J. I. Katz, Phys. Rev. Lett. **78**, 4506 (1997).
[29] J. E. McDonald, Am. J. Phys. **30**, 870 (1962).
[30] J. E. McDonald, Am. J. Phys. **31**, 31 (1963).
[31] I. Napari and H. Vehkamäki, J. Chem. Phys. **124**, 024303 (2006).
[32] I. J. Ford and S. A. Harris, J. Chem. Phys. **120**, 4428 (2004).
[33] J. Barrett, J. Chem. Phys. **116**, 8856 (2002).